

# EGOBRAIN: SYNERGIZING MINDS AND EYES FOR HUMAN ACTION UNDERSTANDING

**Nie Lin<sup>1,\*</sup>, Yansen Wang<sup>2</sup>, Dongqi Han<sup>2</sup>, Weibang Jiang<sup>2</sup>, Jingyuan Li<sup>2</sup>, Ryosuke Furuta<sup>1</sup>, Yoichi Sato<sup>1,†</sup>, Dongsheng Li<sup>2,†</sup>**

<sup>1</sup>The University of Tokyo <sup>2</sup>Microsoft Research Asia

## ABSTRACT

The integration of brain-computer interfaces (BCIs), in particular electroencephalography (EEG), with artificial intelligence (AI) has shown tremendous promise in decoding human cognition and behavior from neural signals. In particular, the rise of multimodal AI models have brought new possibilities that have never been imagined before. Here, we present EgoBrain—the world’s first large-scale, temporally aligned multimodal dataset that synchronizes egocentric vision and EEG of human brain over extended periods of time, establishing a new paradigm for human-centered behavior analysis. This dataset comprises 61 hours of synchronized 32-channel EEG recordings and first-person video from 40 participants engaged in 29 categories of daily activities. We then developed a multimodal learning framework to fuse EEG and vision for action understanding, validated across both cross-subject and cross-environment challenges, achieving an action recognition accuracy of 66.70%. EgoBrain paves the way for a unified framework for brain-computer interface with multiple modalities. All data, tools, and acquisition protocols are openly shared to foster open science in cognitive computing.

## 1 INTRODUCTION

The explosive growth of artificial intelligence has greatly advanced the field of Brain-computer interfaces (BCI), with massive research efforts to understand brain functions from neural recordings. Among various neural signals, non-invasive systems such as scalp electroencephalograph (EEG) are more scalable, cost-effective, and safer for large-scale adoption (Willett et al., 2021; Anumanchipalli et al., 2019; Sivasakthivel et al., 2025; Metzger et al., 2023; Bai et al., 2023; Li et al., 2025; Lan et al., 2023), thus appealing increasing interest to connect EEG with human perceptions and intentions. Boosted by deep learning techniques, booming breakthroughs have been seen in recent years to decode visual and acoustic stimuli in controlled laboratory settings. For example, recent works achieved accuracies of 15.6% in a 200-way zero-shot task on the EEG-image dataset (Song et al., 2023) and 21.9% in a 9-way task on the EEG-video dataset (Liu et al., 2024b). However, the visual stimuli in existing studies were merely presented on screens and the informative environmental background was ignored. Moreover, the active interactions between the subjects and the environment are less explored due to the passive settings in the experiments.

To better capture real-world human perceptions and actions, we introduce egocentric (first-person-view) vision as a complementary modality to EEG. The egocentric vision has emerged as a powerful paradigm for modeling human-object interactions and perceptual processes in real-world settings, with representative large-scale datasets such as EPIC-KITCHENS(Damen et al., 2022), Ego4D(Grauman et al., 2022) and HoloAssist(Wang et al., 2023). These datasets primarily capture observable outcomes from a human-like perspective, yielding valuable analysis of human behavior such as action recognition, hand pose estimation and human-object interaction understanding.

Interestingly, EEG and egocentric vision provide mutually reinforcing information. While the first-person-view video offers objective information about scenes and actions, the sensorimotor experiences, intentions, and other forms of implicit knowledge remain largely unobservable. The missing

\* Work done during an internship at Microsoft. <sup>†</sup> Co-corresponding authors.

pieces can be seamlessly complemented by EEG signals which reveal the latent cognitive signals related to attention, motor planning, decision-making, and intention. Given the complementary nature of egocentric vision and EEG, three fundamental questions arise. First, can their combination lead to a deeper understanding of human behavior? Second, when does this integration outperform unimodal approaches? Third, what technical methodologies can effectively handle the fusion?

To seek the answer and advance human-centric multimodal research, we start from introducing Ego-Brain, a large-scale multimodal dataset that synchronously captures EEG and egocentric video from 40 participants engaged in natural daily activities. With a sophisticated design of 29 actions and diverse environmental conditions in test sets, EgoBrain offers the first benchmark of multimodal action recognition from synchronized EEG and egocentric video, paving the way for a unified framework for brain-computer interface.

Similar to other multimodal tasks with synchronized timeline, it's crucial to handle the shared temporal structure carefully and fuse information from modalities for downstream prediction. Upon our EgoBrain dataset, we present an adaptive Brain-Time Interval Machine (Brain-TIM) model, inspired from (Chalk et al., 2024) to integrate synchronized visual and EEG signals and capture rich multimodal information for action understanding. Each modality is processed through modality-specific embedding layers and merged to the aggregated global context, while the shared temporal structure is explicitly modeled using the Time Interval MLP (TIM) module. We then conducted experiments with our Brain-TIM to evaluate both the standalone effectiveness of individual modalities and their synergy, and the highlighted results confirmed that the fusion of EEG and vision consistently outperforms unimodal approaches across multiple experiments. Further visualization provide deeper insight into the complementary roles of egocentric vision and EEG signals. We summarize our contributions as:

- 1) We introduce EgoBrain, the first large-scale synchronized EEG dataset designed for egocentric vision research. Featuring data from 40 participants engaged in real-world activities such as tool use and daily tasks (in total 61 hours), this dataset sets a benchmark for cross-modal action understanding and advances the application of BCI technologies in real-life settings.
- 2) To lay the groundwork, we provide standardized preprocessing pipelines for vision-brain synchronization data, along with benchmark evaluations and our proposed Brain-TIM model. These resources ensure experimental reproducibility and offer a unified comparative benchmark for future research based on EgoBrain.
- 3) We conduct ablation studies to assess the individual and combined contributions of different modalities. Our findings offer valuable insights into designing cross-modal learning frameworks for egocentric vision and brain signal integration.

## 2 RELATED WORK

**EEG & Vision Integration:** In recent years, combining electroencephalography (EEG) with visual data has emerged as a central theme in brain–computer interface (BCI) research, elucidating cognitive processes and motor intentions(Mushtaq et al., 2024; Guttmann-Flury et al., 2025; Bertoni et al., 2025; Dreyer et al., 2023; Kaya et al., 2018). EEG's high temporal resolution and portability enable real-time monitoring of brain states, yet most work examines resting-state responses to static visual stimuli, neglecting neural dynamics during natural movement(Yang et al., 2025; Liu et al., 2025; Ma et al., 2022; 2020; Liu et al., 2024a). A few studies have recorded EEG during active locomotion—for example, assessing cognitive load while walking in a lower-limb exoskeleton(Ortiz et al., 2023)—and virtual-reality tasks like supernumerary thumb control via motor imagery(Alsuradi et al., 2024). However, these efforts target prosthetic control and lack a systematic exploration of real-world, first-person multimodal interactions in unconstrained movement.

**Egocentric Vision Datasets:** Recent egocentric video corpora have advanced human–object interaction modeling through varied contexts and annotations(Damen et al., 2022; Grauman et al., 2022; Wang et al., 2023; Darkhalil et al., 2022; Kwon et al., 2021; Liu et al., 2022; Ragusa et al., 2021; Sener et al., 2022; Ohkawa et al., 2023; Zhang et al., 2022; Grauman et al., 2024; Huang et al., 2024). EPIC-KITCHENS(Damen et al., 2022) offers detailed kitchen-activity labels, while Ego4D(Grauman et al., 2022) provides the largest in-the-wild egocentric set for 3D perception and social analysis. HoloAssist(Wang et al., 2023) enables multi-user task completion, and Assembly-series(Sener et al., 2022; Ohkawa et al., 2023) and H2O(Kwon et al., 2021) cover procedural and two-hand manipulations. More recent datasets like EgoExoLearn(Huang et al., 2024) and Ego-

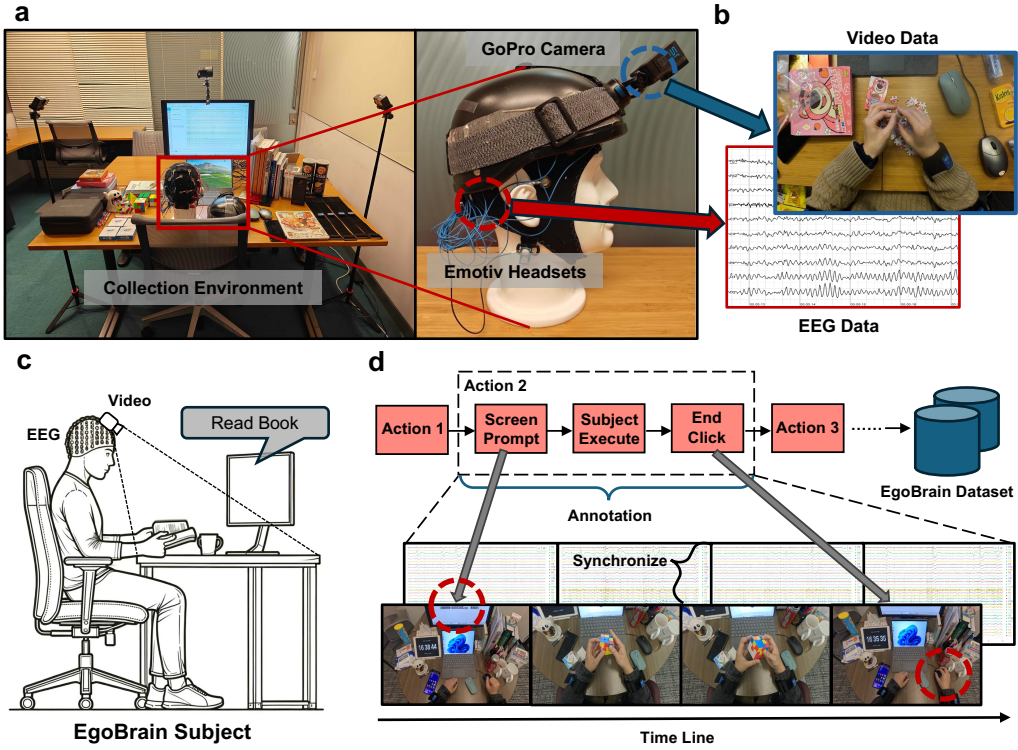


Figure 1: **The EgoBrain dataset and experimental setup.** **a** (Left) Acoustic isolation chamber with adjustable lighting and modular workstation containing standardized interaction objects. (Right) Portable apparatus configuration showing helmet-mounted GoPro camera and Emotive FLEX 2 Gel EEG headset. **b** High-fidelity egocentric video recording hand-object interactions and 32-channel EEG signals. **c** Subject performing (“Read book”) action following on-screen textual prompts. **d** From command display (“Play Cube”) to object interaction and completion confirmation.

Exo4D(Grauman et al., 2024) deliver asynchronous and dual-perspective recordings of skilled activities. Unlike these vision-only resources, our EgoBrain jointly captures first-person video and EEG, facilitating cross-modal action recognition.

Overall, existing research overlooks the synchronization of egocentric visual data and brain activity during dynamic interactions in daily life.

### 3 EGOBRAIN DATASET

**Environment and Data Acquisition System** Fig.1a illustrates our data capture environment within an acoustic isolation chamber. The setup incorporates adjustable lighting and a modular workstation containing standardized objects (books, electronic devices, *etc.*) for controlled interactions. The right panel of Fig. 1a illustrates the configuration of our portable recording apparatus. The setup includes a helmet-mounted GoPro HERO12 camera (1080P/30Hz) for capturing high-quality egocentric video and a 32-channel wireless EEG headset (Emotive FLEX 2 Gel System, 256Hz sampling rate) compliant with the international 10-20 electrode placement standard.

Throughout the session, the participant remains seated to reduce excessive lower-limb movement that may otherwise introduce artifacts into the EEG signals, and the GoPro camera is carefully aligned to the participant’s visual horizon to ensure a natural first-person perspective. The subject is asked to conduct some everyday interaction with the objects illustrated in Fig. 1c. Meanwhile, the data acquisition system captures two key modalities: high-fidelity egocentric video recordings and 32-channel EEG signals, with an example shown in Fig. 1b. Both modalities are time-locked to the execution of these actions, achieved through synchronization with a reference display (<1s jitter).

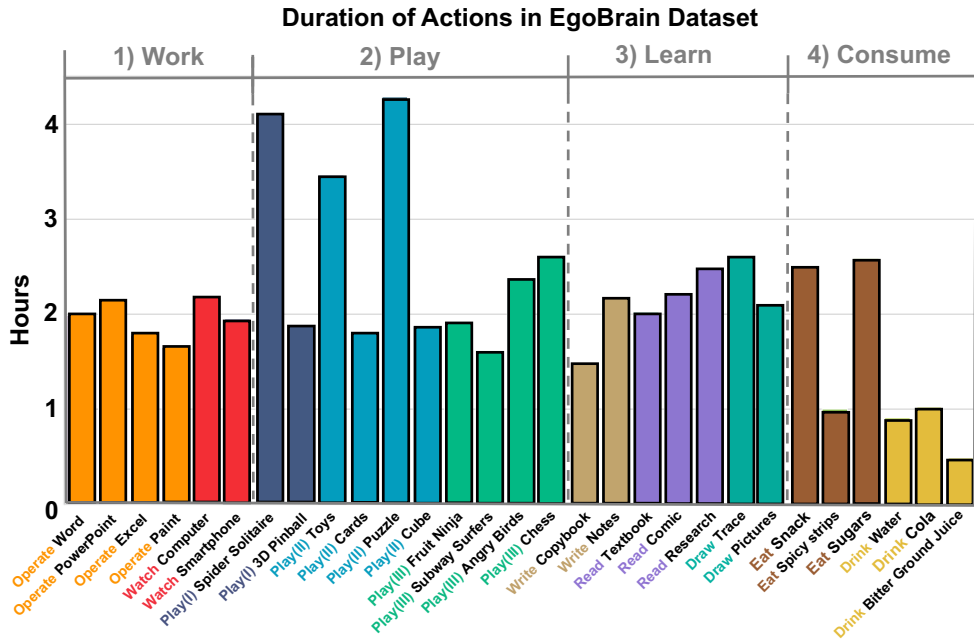


Figure 2: **The EgoBrain statistics.** The total duration per category is presented, highlighting the longest duration (Play(II) puzzle: 4.29 hours) and the shortest duration (Drink Bitter Juice: 0.49 hours)

**Data Acquisition Pipeline** Fig. 1d presents a detailed visualization of our standardized action execution pipeline. A session consists of a predefined yet randomly shuffled sequence of 29 actions, with consume-related actions repeated for three times (narrated in the next section). At the beginning of each action, a large display screen presents a task prompt (e.g., “*Play cube*”). The prompt instructs the subject to identify the relevant object placed on the table, initiate the corresponding hand-object interaction. The completion of a task is marked by the subject successfully performing the interaction and manually confirming it via a mouse click. This human-initiated confirmation ensures the intentional execution and completeness of each action, and naturally results in varying action durations across different tasks. Upon task completion, the system automatically advances to the next predefined action until the subject completes the full set of programmed tasks.

**Action Category Design** The EgoBrain dataset encompasses a broad spectrum of daily activities, covering 29 distinct hand-object interaction tasks, categorized into 10 verbs and 4 major classes:

- **Work Classes:** Tasks such as operating Word, PowerPoint, Excel, and Paint applications.
- **Play Classes:** Activities including computer games, mobile games, puzzles, and cubes.
- **Learn Classes:** Tasks such as writing, reading textbooks, and reading research articles.
- **Consume Classes:** Actions related to eating snacks, drinking water and cola.

These activities span a wide range of temporal scales, with individual task durations ranging from 1,753 seconds (approximately 0.49 hours) to 15,441 seconds (approximately 4.29 hours), reflecting significant diversity in both task complexity. We visualize the cumulative time per activity (in hours) in the left part of Fig. 2.

From a temporal standpoint, the longest-duration activities predominantly fall within the *Play* and *Work* categories. For instance, “*play puzzles*“ demands sustained attention and intricate hand movements, while “*watch computer videos*“ or “*play games*“ can span extended periods. In contrast, actions within the *Consume* category are typically brief and episodic. To mitigate under-representation of such short-duration behaviors, we introduced randomized repetition and each consume-related action was performed three times during data collection to enrich the class distribution.

**Subjects** The dataset includes recordings from a total of 40 participants, with a gender ratio of 27 male to 13 female subjects. All subjects were informed of the experimental process and signed informed consent forms before the experiment. This study was approved by the ethical committee of local Institutional Review Board for Human Research Protections.

**Data Split** We divide the dataset into training, validation, and test sets following the standard data split protocol. To increase the evaluation challenge of the EgoBrain dataset, we design two splits of different difficulty gradient, namely the Cross-Subject-Only split and the Cross-Subject&Cross-Scene split.

For the Cross-Subject-Only setting, we collected 34 sessions from different subjects within the same physical location and object arrangement. The 34 subjects are divided into train set with 22 subjects (32.96 hours), validation set with 6 subjects (7.75 hours), and test set with remaining 6 subjects (9.08 hours).

For the Cross-Subject&Cross-Scene split, besides the 34 sessions, we collected 6 more sessions in another laboratory, with the same data collection protocol, similar object arrangement, but totally different background environment. The train set and validation set consists of 28 subjects (40.71 hours) and 6 subjects (9.08 hours), and the 6 more sessions (11.28 hours) in the new environment constitutes the test set, assuring that the new environment is never seen during the training and validation stage.

## 4 METHODS

After constructing the EgoBrain dataset, we detail how we build an effective framework, namely Brain-TIM, to model these multimodal temporal inputs to address the action understanding task.

### 4.1 TASK DEFINITION

We consider a time-synchronized pair of raw data: the egocentric video stream and the EEG signal sequence, both sharing a common timeline  $\mathcal{T} = [0, T]$ . The video stream is represented as  $V^{\text{raw}} = \{v_t \in \mathbb{R}^{H \times W \times 3}\}_{t=0}^{T \cdot f^v}$ , sampled at a frame rate  $f^v$ , and the EEG signal as  $B^{\text{raw}} = \{b_t \in \mathbb{R}^C\}_{t=0}^{T \cdot f^b}$ , recorded at  $f^b$  Hz, where  $C$  is the number of channels. The target of action recognition task can be formulated as finding the best mapping from input to the action and verb categories  $\hat{y} = f_\theta(V, B) \in \{1, \dots, N_c\}^Q$ , where  $N_c$  equals to 10 for verb classification or 29 for action categories, and  $Q$  is the number of consecutive queries which evenly divides the whole time interval  $[0, T]$ , i.e, the  $i$ -th query corresponds to the action within time  $[(i-1)T/Q, iT/Q]$ .

### 4.2 OVERVIEW OF BRAIN-TIM

An overview of Brain-TIM is presented in Fig. 3. We first extract feature representations for each modality using pre-trained backbone networks (Tong et al., 2022; Jiang et al., 2024) into  $\phi^v$  and  $\phi^b$  (Appendix A.1). These features are then projected into a shared embedding space via modality-specific embedding layers:  $g^v$  and  $g^b$  (Appendix A.2). The embeddings from different modalities are concatenated to form a unified input sequence for the Transformer module on the right side of the Fig. 3 (Appendix A.2). Eventually, the Transformer encoder models the temporal dependencies and cross-modal interactions within the sequence (Appendix A.3) and a linear classifier maps the encoded features to the final action category predictions (Appendix A.4).

### 4.3 SEQUENCE CONCATENATION WITH TEMPORAL AND MODALITY-SPECIFIC INFORMATION

To discriminate tokens before feeding them into transformer and enhance the representations with temporal and modality-specific information, we introduce the Time-aware Token Embedding and the Modality-specific embedding following (Chalk et al., 2024).

**Time-aware Token Embedding:** To incorporate the time-specific information to the tokens, we explicitly add it by introducing the Time-Interval MLP (TIM),  $I(\cdot) : \mathbb{R}^2 \rightarrow \mathbb{R}^D$ , consisting of three

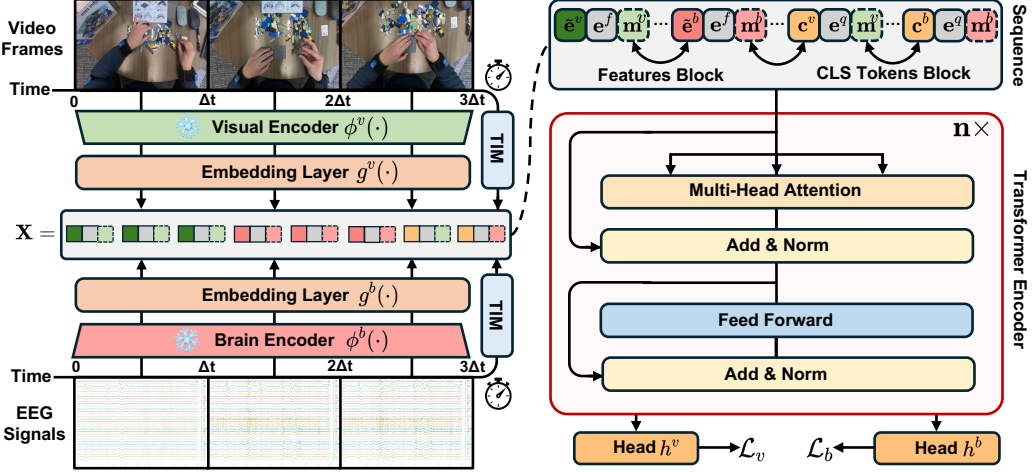


Figure 3: The overall architecture of Brain-TIM. The model processes synchronized visual and EEG signals using modality-specific encoders, followed by embedding layers to obtain token sequences. The shared temporal axis is concurrently encoded by the TIM module. A modality-aware CLS token is appended to the sequence to capture global semantics. The resulting tokens are fed into a Transformer encoder for downstream action classification.

linear layers with ReLU activations and LayerNorm operation. This TIM module takes the start and end time ( $t_s, t_e$ ) of the corresponding interval as input and generate the temporal embedding which can be further appended to the specific token as a time-aware token embedding.

For the feature tokens  $\tilde{e}_i^v$  and  $\tilde{e}_i^b$ , the time interval is determined by the  $i$ -th window  $[t_i, t_i + \Delta t]$ , also named feature time in (Chalk et al., 2024). The temporal embedding is thus calculated as  $\mathbf{e}_i^f = I(t_i, t_i + \Delta t) \in \mathbb{R}^D$ . As for the CLS tokens  $\mathbf{c}_j^v$  and  $\mathbf{c}_j^b$ , the time interval corresponds to the  $j$ -th query  $[(j-1)T/Q, jT/Q]$ , also known as query time. And the temporal embedding is similarly obtained as  $\mathbf{e}_j^q = I((j-1)T/Q, jT/Q) \in \mathbb{R}^D$ .

**Modality-specific Embedding:** To distinguish tokens of different modality, we further introduced the modality-specific embedding, represented by two learnable vectors,  $\mathbf{m}^v \in \mathbb{R}^{2D}$  and  $\mathbf{m}^b \in \mathbb{R}^{2D}$ , to store shared vision-modality and EEG-modality information, respectively. The modality-specific embeddings are directly added to the tokens of corresponding modality.

**Sequence Concatenation:** The input sequence to the transformer encoder is obtained as follows:

$$\mathbf{X} = \text{Concat}\left(\underbrace{\{\tilde{e}_i^v \parallel \mathbf{e}_i^f + \mathbf{m}^v\}_{i=1}^N}_{\text{visual feature block}}, \underbrace{\{\tilde{e}_i^b \parallel \mathbf{e}_i^f + \mathbf{m}^b\}_{i=1}^N}_{\text{brain feature block}}, \underbrace{\{\mathbf{c}_j^v \parallel \mathbf{e}_j^q + \mathbf{m}^v\}_{j=1}^Q}_{\text{visual CLS token block}}, \underbrace{\{\mathbf{c}_j^b \parallel \mathbf{e}_j^q + \mathbf{m}^b\}_{j=1}^Q}_{\text{brain CLS token block}}\right),$$

where each element is constructed by concatenating the original token with its temporal embedding, added to the modality-specific embedding. This final input sequence  $\mathbf{X} \in \mathbb{R}^{(2N+2Q) \times 2D}$  is formed by orderly concatenating all processed feature representations and CLS tokens.

This design offers three key advantages: 1) it ensures cross-modal time-aware alignment through shared temporal encodings; 2) preserves modality-specific characteristics by utilizing independent modality embeddings; and 3) facilitates cross-modal interaction and query-specific classification by implementing symmetric handling of CLS tokens.

## 5 EXPERIMENTAL RESULTS

We rephrase the research questions proposed in the introduction here:

**RQ1:** Does a combination of egocentric video and EEG enable a more comprehensive understanding of human behavior?

**RQ2:** Is our proposed method effective for this multimodal action recognition task?

**RQ3:** When does this integration outperform unimodal approaches?

Table 1: **Action recognition results on the EgoBrain test set.** We systematically evaluate unimodal (Brain only, Visual only) and multimodal (Visual+Brain) models under two protocols: **cross-subject only** and **cross-subject & cross-scene**. The table reports the parameter scale (Params) of each model and the mean  $\pm$  standard deviation across five random seeds to ensure statistical reliability. The primary evaluation metric is Top-1 accuracy (%), with the best results highlighted in **bold**.

Protocol	Modality	Encoder	Params	Verb Acc. %	Action Acc. %
Cross-subject only	Brain only	LaBraM (Jiang et al., 2024)	<b>5.8M</b>	$21.53 \pm 0.99$	$8.44 \pm 2.25$
	Visual only	VideoMAE (Tong et al., 2022)	<b>305.0M</b>	$88.95 \pm 0.80$	$78.44 \pm 0.71$
	Visual + Brain	VideoMAE + LaBraM (Tong et al., 2022; Jiang et al., 2024)	<b>310.8M</b>	<b><math>90.11 \pm 1.10</math></b>	<b><math>80.16 \pm 1.67</math></b>
Cross-subject & Cross-scene	Brain only	LaBraM (Jiang et al., 2024)	<b>5.8M</b>	$19.41 \pm 1.57$	$9.36 \pm 0.52$
	Visual only	VideoMAE (Tong et al., 2022)	<b>305.0M</b>	$81.67 \pm 1.89$	$63.40 \pm 0.95$
	Visual + Brain	VideoMAE + LaBraM (Tong et al., 2022; Jiang et al., 2024)	<b>310.8M</b>	<b><math>83.43 \pm 0.41</math></b>	<b><math>66.70 \pm 0.83</math></b>

We designed comprehensive experiments to answer these research questions in this section.

### 5.1 ACTION CLASSIFICATION RESULTS ON EGOBRAIN

We evaluate Brain-TIM on test sets of the EgoBrain dataset (Tab. 1) to answer **RQ1**. Note that all experimental results presented in the tables are Mean  $\pm$  STD across five different random seeds.

**Unimodal Comparison:** As a well-studied computer vision problem, the visual modality demonstrates significantly strong performance, achieving 88.95% Top-1 accuracy for verb classification and 78.44 % for action classification in the cross-subject setting. Thanks to its superior spatial resolution and contextual richness, egocentric visual input provides fine-grained cues that are critical for distinguishing actions and achieved the performances of 81.67% and 63.40% for verb and action classification even under the challenging cross-subject and cross-scene settings.

As for the EEG modality, the model achieves relatively low yet significantly better performance than chance level for both settings. While EEG data contains certain cognitive information, its relatively low sampling rate and limited feature dimensionality restrict its effectiveness in complex real-world scenarios applied individually.

**Multimodal Comparison:** As shown in Tab. 1, fusing EEG with visual inputs boosts accuracies across both evaluation protocols. Under the cross-subject only setting, the vision-only baseline achieves 78.44% Top-1 accuracy for action classification, while Brain-TIM reaches 80.16%, giving a 1.72% improvement. Specifically, under the most difficult cross-scene setting, the vision-only baseline achieves 63.40% Top-1 accuracy for action classification, while Brain-TIM with both modalities reaches 66.70%, yielding a 3.30% absolute improvement on the 29-class task. This performance gain answers **RQ1** and further highlights the semantic complementarity between the two modalities: while the visual stream captures external manifestations of action, EEG encodes neural signatures of motor intention and implicit knowledge that are not observable from eyes alone.

Importantly, the performance gains of EEG are not attributable to differences in model capacity, but rather to its unique cognitive value. Our EEG encoder is extremely lightweight, with only 5.8M parameters (approximately 1/52 of the visual backbone), yet it still delivers statistically significant improvements. This demonstrates that EEG provides indispensable complementary information in cases of visual ambiguity or occlusion, thereby rendering visual understanding more complete.

### 5.2 ABLATION STUDY

To answer **RQ2** and see whether all the proposed techniques are positively contributing to the decoding task, we removed some components from Brain-TIM and conducted ablation study.

Table 2: **Ablation results of Brain-TIM.** The results show the effects of key modules under Brain Only, Visual Only, and combined Visual & Brain settings.

	Brain Only				Visual Only				Visual & Brain			
Embedding Layer $g^{(v,b)}$	<span style="color:red">X</span>	<span style="color:green">✓</span>	<span style="color:red">X</span>	<span style="color:green">✓</span>	<span style="color:red">X</span>	<span style="color:green">✓</span>	<span style="color:red">X</span>	<span style="color:green">✓</span>	<span style="color:red">X</span>	<span style="color:green">✓</span>	<span style="color:red">X</span>	<span style="color:green">✓</span>
Time Interval MLP $I^{(v,b)}$	<span style="color:red">X</span>	<span style="color:red">X</span>	<span style="color:green">✓</span>	<span style="color:green">✓</span>	<span style="color:red">X</span>	<span style="color:red">X</span>	<span style="color:green">✓</span>	<span style="color:green">✓</span>	<span style="color:red">X</span>	<span style="color:red">X</span>	<span style="color:green">✓</span>	<span style="color:green">✓</span>
Modality Embedding $m^{(v,b)}$												
Action Acc. % @Top-1 Mean	7.44	—	7.54	6.15	<b>9.36</b>	<b>64.94</b>	64.67	64.01	63.40	65.71	65.81	66.39
Action Acc. % @Top-1 STD	0.39	0.05	0.06	0.52	3.64	1.75	6.34	0.95	0.43	2.15	0.09	2.22
												66.18
												<b>66.70</b>
												0.83

Table 2 presents the performance under three modality settings: Brain Only, Visual Only, and Visual & Brain. For each setting, we evaluate different combinations of three key components: the embedding layer  $g^{(v,b)}$ , the time interval MLP  $I^{(v,b)}$ , and the modality embedding  $m^{(v,b)}$ .

To conclude, all the components help boost the performance for the action recognition task in the pure EEG setting and the multimodal setting, indicating the effectiveness of the embedding layer to enhance representations, the time interval MLP to incorporate temporal features, and the modality embedding to keep modality-specific information. It's also interesting to see that the extra designs will harm the final performance in the vision-only setting, as we guess the vision modality is enough for stand-alone predictions and adding more information will introduce undesired parameters, adding obstacles to the training process.

### 5.3 DETAILED ANALYSIS

To answer **RQ3**, we dive into the specific categories and cases to see when the multimodal framework outperforms the unimodal cases.

**Confusion Matrix of Classification:** We present in Fig. 4 the confusion matrices comparing unimodal (visual-only) and multimodal (visual + EEG) models for verb classification. To assess the impact of multimodal fusion, verbs are grouped into two clusters: “Work”/“Play” on the left, and “Learn”/“Consume” on the right. Comparing Fig. 4a (visual-only) and Fig. 4b (visual + EEG) reveals that EEG integration does not uniformly improve all categories. Notable improvements are seen in “Play(I)” ( $0.46 \rightarrow 0.64$ ), suggesting EEG complements cognitively demanding actions. The “Drink” category benefits from EEG under visual occlusion ( $0.87 \rightarrow 0.94$ ). However, “Write” accuracy decreases ( $0.83 \rightarrow 0.77$ ), likely due to kinematic redundancy, where EEG introduces noise in cases of clear visual motion patterns. These results indicate EEG’s compensatory effect is task-dependent, offering marginal gains when visual cues are strong.

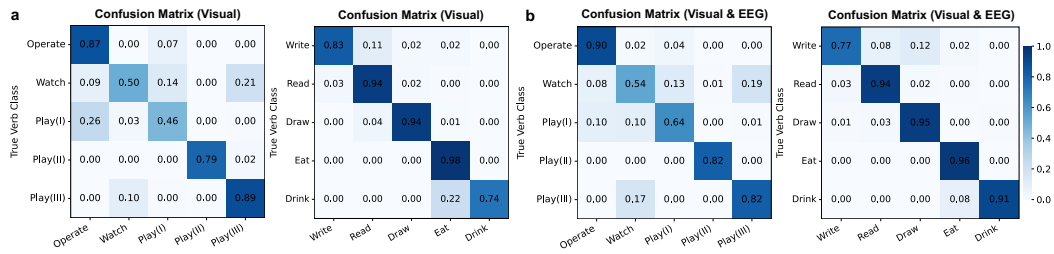
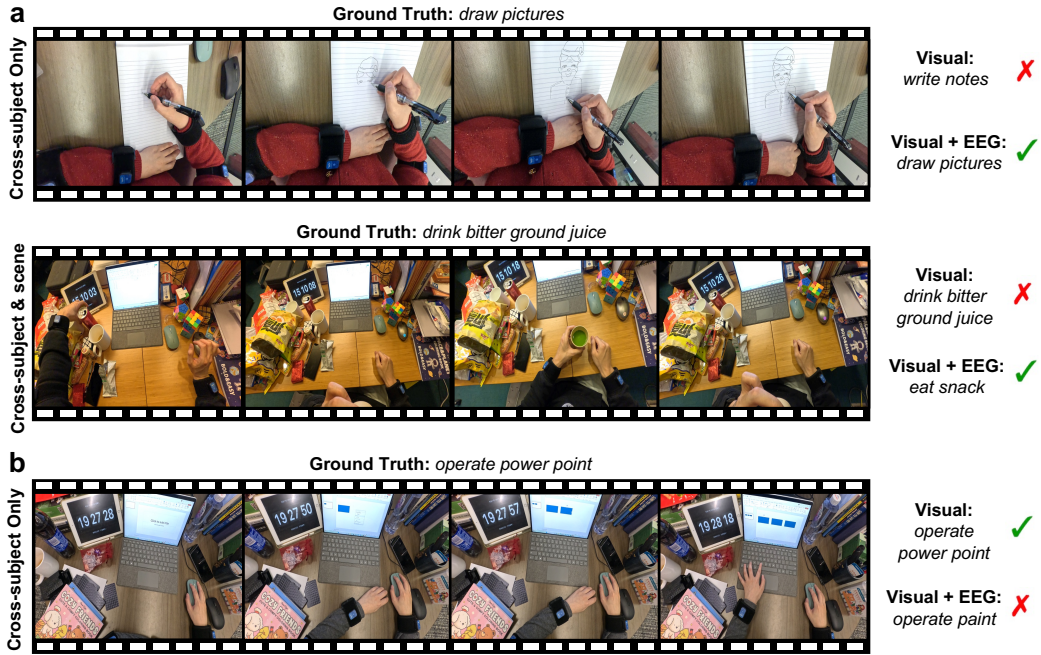


Figure 4: **Confusion matrix for verb classification: unimodal vs. multimodal.** **a** Visual-only classification. **b** Visual-EEG fusion. EEG improves “Play(I)” accuracy ( $0.46 \rightarrow 0.64$ ), and boosts “Drink” ( $0.87 \rightarrow 0.94$ ), showing its essential role when vision information is vague.

We further elucidate the behavior of our multimodal model, we present representative examples of both successful and failed cases in Fig.5. Panels (a) and (b) illustrate two typical scenarios: instances where EEG signals enhance performance and cases where EEG introduces errors.

**Benefits of Integrating EEG:** As shown in Fig.5a, when a participant is drawing in a notebook, the visual model misclassifies the action as “writing” due to the high visual similarity between the two tasks. However, after incorporating EEG data, the model correctly classifies the action as “drawing”. This suggesting that EEG signals may capture neural patterns related to task intent and



**Figure 5: Success and Failure Cases for Unimodal (Visual) and Multimodal (Visual + EEG) Models.** (a) Multimodal model correctly recognizes actions that the visual-only model misses, aided by EEG. (b) EEG causes misclassification, possibly due to overlapping cognitive strategies.

offer additional discriminative cues. This suggests that EEG captures distinct neural activations associated with visuospatial motor planning as opposed to language-related tasks—a distinction that has been well documented in prior neuroscience studies(Tang et al., 2024).

Another example in Fig.5a involves the action of “*drink - bitter ground juice*”. Due to occlusion, the subject’s hand and the cup are not visible, and the visual model misclassifies the action as “*snack*” based on nearby contextual visual cues (e.g., a bag of chips). With EEG integration, the model not only correctly identifies the verb “*drink*” but also the object “*bitter melon juice*”. This improvement likely stems from EEG’s ability to reflect orofacial motor patterns and anticipatory neural activity related to swallowing, which differ from those associated with chewing(Saito et al., 2024). The results underscore EEG’s value in disambiguating semantically similar actions when vision is limited.

**Limitations of Integrating EEG:** Despite these advantages, EEG does not always lead to improved recognition. Fig.5b presents failure cases of the multimodal model. The participant is actually operating PowerPoint, but the model incorrectly identifies the task as using a drawing application. Possible reason is that the participant is creating multiple rectangles, evoking visuomotor activity patterns that resemble those during freehand drawing. Prior studies have shown that such overlapping cognitive strategies lead to similar EEG signatures(Dvorak et al., 2018), making semantic discrimination harder.

## 6 CONCLUSION AND DISCUSSION

We draw on the metaphor that “*the eyes are the windows to the mind*” to argue that egocentric video can illuminate neural states that EEG alone cannot. Despite its promise, no dataset or systematic study has yet explored EEG–vision synergy in real-world tasks. We construct EgoBrain, the first action understanding dataset that simultaneously captures first-person video and EEG signals, aiming to advance research on vision-brain signal integration. We further develop Brain-TIM as the first multimodal research baseline on EgoBrain. Experimental results show that combining EEG and visual modalities significantly outperforms single-modality approaches, highlighting the potential of multimodal modeling in complex cognitive scenarios. Notably, we find that EEG signals offer

critical complementary information to vision, particularly in scenarios with limited *e.g.*, drinking) or ambiguous (*e.g.*, writing vs. drawing) visual cues.

Our work lays the foundation for applying multimodal brain–computer interfaces to high-level cognitive tasks by introducing a new visuo-neural dataset and an efficient benchmark model. We believe that they will open up the new possibility for brain-vision multimodal learning, and we anticipate future works to actively explore the interaction mechanisms between visual and neural modalities and ignite discovering new tasks.

## REFERENCES

H. Alsuradi, J. Hong, A. Sarmadi, R. Volcic, H. Salam, S. F. Atashzar, F. Khorrami, and M. Eid. Neural signatures of motor imagery for a supernumerary thumb in vr: an eeg analysis. *Scientific Reports*, 14:21558, 2024. doi: 10.1038/s41598-024-72358-3.

G. K. Anumanchipalli, J. Chartier, and E. F. Chang. Speech synthesis from neural decoding of spoken sentences. *Nature*, 568:493–498, 2019. doi: 10.1038/s41586-019-1119-1.

Y. Bai, X. Wang, Y. p. Cao, Y. Ge, C. Yuan, and Y. Shan. Dreamdiffusion: Generating high-quality images from brain eeg signals. *arXiv preprint arXiv:2306.16934*, 2023.

T. Bertoni, J. P. Noel, M. Bockbrader, C. Foglia, S. Colachis, B. Orset, N. Evans, B. Herbelin, A. Rezai, S. Panzeri, C. Becchio, O. Blanke, and A. Serino. Pre-movement sensorimotor oscillations shape the sense of agency by gating cortical connectivity. *Nature Communications*, 16: 3594, 2025. doi: 10.1038/s41467-025-58683-9.

J. Chalk, J. Huh, E. Kazakos, A. Zisserman, and D. Damen. TIM: A Time Interval Machine for Audio-Visual Action Recognition. In *Proceedings of the IEEE/CVF Conference on Computer Vision and Pattern Recognition (CVPR)*, pp. 18153–18163, 2024.

D. Damen, H. Doughty, G. M. Farinella, A. Furnari, J. Ma, E. Kazakos, D. Moltisanti, J. Munro, T. Perrett, W. Price, and M. Wray. Rescaling egocentric vision: Collection, pipeline and challenges for epic-kitchens-100. *International Journal of Computer Vision (IJCV)*, 130(1):33–55, 2022.

A. Darkhalil, D. Shan, B. Zhu, J. Ma, A. Kar, R. E. L. Higgins, S. Fidler, D. Fouhey, and D. Damen. EPIC-KITCHENS VISOR benchmark: Video segmentations and object relations. In *Proceedings of the Neural Information Processing Systems (NeurIPS) Track on Datasets and Benchmarks*, 2022.

J. Deng, W. Dong, R. Socher, L.-J. Li, K. Li, and L. Fei-Fei. Imagenet: A large-scale hierarchical image database. In *Proceedings of the IEEE/CVF Conference on Computer Vision and Pattern Recognition (CVPR)*, pp. 248–255, 2009.

P. Dreyer, A. Roc, L. Pillette, S. Rimbert, and F. Lotte. A large eeg database with users’ profile information for motor imagery brain-computer interface research. *Scientific Data*, 10:580, 2023. doi: 10.1038/s41597-023-02445-z.

D. Dvorak, A. Shang, S. Abdel-Baki, W. Suzuki, and A. A. Fenton. Cognitive behavior classification from scalp eeg signals. *IEEE Transactions on Neural Systems and Rehabilitation Engineering*, 26(4):729–739, 2018.

K. Grauman, A. Westbury, E. Byrne, Z. Chavis, A. Furnari, R. Girdhar, J. Hamburger, H. Jiang, M. Liu, X. Liu, M. Martin, T. Nagarajan, I. Radosavovic, S. K. Ramakrishnan, F. Ryan, J. Sharma, M. Wray, M.g Xu, E. Zhongcong Xu, C. Zhao, S. Bansal, D. Batra, V. Cartillier, S. Crane, T. Do, M. Doulaty, A. Erappalli, C. Feichtenhofer, A. Fragomeni, Q. Fu, C. Fuegen, A. Gebreselasie, C. Gonzalez, J. Hillis, X. Huang, Y. Huang, W. Jia, W. Khoo, J. Kolar, S. Kottur, A. Kumar, F. Landini, C. Li, Y. Li, Z. Li, K. Mangalam, R. Modhugu, J. Munro, T. Murrell, T. Nishiyasu, W. Price, P. R. Puentes, M. Ramazanova, L. Sari, K. Somasundaram, A. Southerland, Y. Sugano, R. Tao, M. Vo, Y. Wang, X. Wu, T. Yagi, Y. Zhu, P. Arbelaez, D. Crandall, D. Damen, G. M. Farinella, B. Ghanem, V. K. Ithapu, C. V. Jawahar, H. Joo, K. Kitani, H. Li, R. Newcombe, A. Oliva, H. Soo Park, J. M. Rehg, Y. Sato, J. Shi, M. Z. Shou, A. Torralba, Lo Torresani, M.i

Yan, and J. Malik. Ego4D: Around the world in 3,000 hours of egocentric video. In *Proceedings of the IEEE/CVF Conference on Computer Vision and Pattern Recognition (CVPR)*, pp. 18973–18990, 2022.

K. Grauman, A. Westbury, L. Torresani, K. Kitani, J. Malik, T. Afouras, K. Ashutosh, V. Baiyya, S. Bansal, B. Boote, E. Byrne, Z. Chavis, J. Chen, F. Cheng, F.-J. Chu, S. Crane, A. Dasgupta, J. Dong, M. Escobar, C. Forigu, A. Gebreselasie, S. Haresh, J. Huang, M. M. Islam, S. D. Jain, R. Khirodkar, D. Kukreja, K. J. Liang, J.-W. Liu, S. Majumder, Y. Mao, M. Martin, E. Mavroudi, T. Nagarajan, F. Ragusa, S. K. Ramakrishnan, L. Seminara, A. Somayazulu, Y. Song, S. Su, Z. Xue, E. Zhang, J. Zhang, A. Castillo, C. Chen, X. Fu, R. Furuta, C. González, P. Gupta, J. Hu, Y. Huang, Y. Huang, W. Khoo, and et al. Ego-exo4d: Understanding skilled human activity from first- and third-person perspectives. In *Proceedings of the IEEE/CVF Conference on Computer Vision and Pattern Recognition (CVPR)*, pp. 19383–19400, 2024.

E. Guttmann-Flury, X. Sheng, and X. Zhu. Dataset combining eeg, eye-tracking, and high-speed video for ocular activity analysis across bci paradigms. *Scientific Data*, 12:587, 2025. doi: 10.1038/s41597-025-04861-9.

Y. Huang, G. Chen, J. Xu, M. Zhang, L. Yang, B. Pei, H. Zhang, D. Lu, Y. Wang, L. Wang, and Y. Qiao. Egoexolearn: A dataset for bridging asynchronous ego- and exo-centric view of procedural activities in real world. In *Proceedings of the IEEE/CVF Conference on Computer Vision and Pattern Recognition (CVPR)*, pp. 22072–22086, 2024.

W. Jiang, L. Zhao, and B. Lu. Large brain model for learning generic representations with tremendous EEG data in BCI. In *Proceedings of the International Conference on Learning Representations (ICLR)*, 2024.

M. Kaya, M. Binli, E. Ozbay, H. Yanar, and Y. Mishchenko. A large electroencephalographic motor imagery dataset for electroencephalographic brain computer interfaces. *Scientific Data*, 5:180211, 2018. doi: 10.1038/sdata.2018.211.

T. Kwon, B. Tekin, J. Stühmer, F. Bogo, and M. Pollefeys. H2O: two hands manipulating objects for first person interaction recognition. In *Proceedings of the IEEE/CVF International Conference on Computer Vision (ICCV)*, pp. 10118–10128, 2021.

Y.-T. Lan, K. Ren, Y. Wang, W.-L. Zheng, D. Li, B.-L. Lu, and L. Qiu. Seeing through the brain: Image reconstruction of visual perception from human brain signals. *arXiv preprint arXiv:2308.02510*, 2023.

J. Li, Y. Wang, N. Lin, and D. Li. Translating mental imaginations into characters with code-books and dynamics-enhanced decoding. In *Proceedings of the IEEE International Conference on Acoustics, Speech and Signal Processing (ICASSP)*. IEEE, 2025.

H. Liu, P. Wei, H. Wang, X. Lv, W. Duan, M. Li, Y. Zhao, Q. Wang, X. Chen, G. Shi, B. Han, and J. Hao. An eeg motor imagery dataset for brain computer interface in acute stroke patients. *Scientific Data*, 11:131, 2024a. doi: 10.1038/s41597-023-02787-8.

X. Liu, Y. Liu, Y. Wang, K. Ren, H. Shi, Z. Wang, D. Li, B. Lu, and W. Zheng. Eeg2video: Towards decoding dynamic visual perception from eeg signals. *Proceedings of the Advances in Neural Information Processing Systems (NeurIPS)*, pp. 72245–72273, 2024b.

Y. Liu, Y. Liu, C. Jiang, K. Lyu, W. Wan, H. Shen, B. Liang, Z. Fu, H. Wang, and L. Yi. Hoi4d: A 4d egocentric dataset for category-level human-object interaction. In *Proceedings of the IEEE/CVF Conference on Computer Vision and Pattern Recognition (CVPR)*, pp. 21013–21022, 2022.

Y. Liu, Z. Gui, D. Yan, Z. Wang, R. Gao, N. Han, J. Chen, J. Wu, and D. Ming. Lower limb motor imagery eeg dataset based on the multi-paradigm and longitudinal-training of stroke patients. *Scientific Data*, 12:314, 2025. doi: 10.1038/s41597-025-04618-4.

J. Ma, B. Yang, W. Qiu, Y. Li, S. Gao, and X. Xia. A large eeg dataset for studying cross-session variability in motor imagery brain-computer interface. *Scientific Data*, 9:531, 2022. doi: 10.1038/s41597-022-01647-1.

X. Ma, S. Qiu, and H. He. Multi-channel eeg recording during motor imagery of different joints from the same limb. *Scientific Data*, 7:191, 2020. doi: 10.1038/s41597-020-0535-2.

S. L. Metzger, K. T. Littlejohn, A. B. Silva, D. A. Moses, M. P. Seaton, R. Wang, M. E. Dougherty, J. R. Liu, P. Wu, M. A. Berger, I. Zhuravleva, A. Tu-Chan, K. Ganguly, G. K. Anumanchipalli, and E. F. Chang. A high-performance neuroprosthesis for speech decoding and avatar control. *Nature*, 620(7976):1037–1046, 2023.

F. Mushtaq, D. Welke, A. Gallagher, Y. G. Pavlov, L. Kouara, J. Bosch-Bayard, J. J. F. van den Bosch, M. Arvaneh, A. R. Bland, M. Chaumon, C. Borck, X. He, S. J. Luck, M. G. Machizawa, C. Pernet, A. Puce, S. J. Segalowitz, C. Rogers, M. Awais, C. Babiloni, N. W. Bailey, S. Baillet, R. C. A. Bendall, D. Brady, M. L. Bringas-Vega, N. A. Busch, A. Calzada-Reyes, A. Chatard, P. E. Clayson, M. X. Cohen, J. Cole, M. Constant, A. Corneyllie, D. Coyle, D. Cruse, I. Delis, A. Delorme, D. Fair, T. H. Falk, M. Gamer, G. Ganis, K. Gloy, S. Gregory, C. D. Hassall, K. E. Hiley, R. B. Ivry, K. Jerbi, M. Jenkins, J. Kaiser, A. Keil, R. T. Knight, S. Kochen, B. Kotchoubey, O. E. Krigolson, N. Langer, H. R. Liesefeld, S. Lippé, R. E. London, A. MacNamara, S. Makeig, W. Marinovic, E. Martínez-Montes, A. A. Marzuki, R. K. Mathew, C. Michel, J. d. R. Millán, M. Mon-Williams, L. Morales-Chacón, R. Naar, G. Nilsonne, G. Niso, E. Nyhus, R. Oostenveld, K. Paul, W. Paulus, D. M. Pfabigan, G. Pourtois, S. Rampp, M. Rausch, K. Robbins, P. M. Rossini, M. Ruzzoli, B. Schmidt, M. Senderecka, N. Srinivasan, Y. Stegmann, P. M. Thompson, M. Valdes-Sosa, M. J. W. van der Molen, D. Veniero, E. Verona, B. Voytek, D. Yao, A. C. Evans, and P. Valdes-Sosa. One hundred years of eeg for brain and behaviour research. *Nature Human Behaviour*, 8:1437–1443, 2024. doi: 10.1038/s41562-024-01941-5.

T. Ohkawa, K. He, F. Sener, T. Hodan, L. Tran, and C. Keskin. AssemblyHands: Towards egocentric activity understanding via 3D hand pose estimation. In *Proceedings of the IEEE/CVF Conference on Computer Vision and Pattern Recognition (CVPR)*, pp. 12999–13008, 2023.

M. Ortiz, L. de la Ossa, J. Juan, E. Iáñez, D. Torricelli, J. Tornero, and J. M. Azorín. An eeg database for the cognitive assessment of motor imagery during walking with a lower-limb exoskeleton. *Scientific Data*, 10:343, 2023. doi: 10.1038/s41597-023-02243-7.

F. Ragusa, A. Furnari, S. Livatino, and G. M. Farinella. The MECCANO dataset: Understanding human-object interactions from egocentric videos in an industrial-like domain. In *Proceedings of the IEEE/CVF Winter Conference on Applications of Computer Vision (WACV)*, pp. 1568–1577, 2021.

N. Saito, T. Ogawa, N. Shiraishi, R. Koide, H. Komine, M. Yokoyama, S. Hanawa, and K. Sasaki. Difference in the electromyographic behavior of the masticatory and swallowing muscles during cued versus spontaneous swallowing. *Dysphagia*, 39(3):398–406, 2024. doi: 10.1007/s00455-024-10031-1.

F. Sener, D. Chatterjee, D. Shelepor, K. He, D. Singhania, R. Wang, and A. Yao. Assembly101: A large-scale multi-view video dataset for understanding procedural activities. In *Proceedings of the IEEE/CVF Conference on Computer Vision and Pattern Recognition (CVPR)*, pp. 21096–21106, 2022.

R. Sivasakthivel, M. Rajagopal, G. Anitha, K. Loganathan, M. Abbas, A. Ksibi, and K. S. Rao. Simulating online and offline tasks using hybrid cheetah optimization algorithm for patients affected by neurodegenerative diseases. *Scientific Reports*, 15:8951, 2025. doi: 10.1038/s41598-025-93047-9.

Y. Song, B. Liu, X. Li, N. Shi, Y. Wang, and X. Gao. Decoding natural images from eeg for object recognition. *arXiv preprint arXiv:2308.13234*, 2023.

J. Tang, Y. Yang, Q. Zhao, Y. Ding, J. Zhang, Y. Song, and W. Kong. Visual guided dual-spatial interaction network for fine-grained brain semantic decoding. *IEEE Transactions on Instrumentation and Measurement*, 2024. doi: 10.1109/TIM.2024.3480232.

Z. Tong, Y. Song, J. Wang, and L. Wang. VideoMAE: Masked autoencoders are data-efficient learners for self-supervised video pre-training. In *Proceedings of the Advances in Neural Information Processing Systems (NeurIPS)*, pp. 10078–10093, 2022.

A. Vaswani, N. Shazeer, N. Parmar, J. Uszkoreit, L. Jones, A. N. Gomez, Ł. Kaiser, and I. Polosukhin. Attention is all you need. In *Proceedings of the Advances in Neural Information Processing Systems (NeurIPS)*, 2017.

X. Wang, T. Kwon, M. Rad, B. Pan, I. Chakraborty, S. Andrist, D. Bohus, A. Feniello, B. Tekin, F. Vieira Frujeri, N. Joshi, and M. Pollefeys. Holoassist: an egocentric human interaction dataset for interactive AI assistants in the real world. In *Proceedings of the IEEE/CVF International Conference on Computer Vision (ICCV)*, pp. 20213–20224, 2023.

F. R. Willett, D. T. Avansino, L. R. Hochberg, J. M. Henderson, and K. V. Shenoy. High-performance brain-to-text communication via handwriting. *Nature*, 593:249–254, 2021. doi: 10.1038/s41586-021-03506-2.

B. Yang, F. Rong, Y. Xie, D. Li, J. Zhang, F. Li, G. Shi, and X. Gao. A multi-day and high-quality eeg dataset for motor imagery brain-computer interface. *Scientific Data*, 12(1):488, 2025. doi: 10.1038/s41597-025-04826-y.

S. Zhang, Q. Ma, Y. Zhang, Z. Qian, T. Kwon, M. Pollefeys, F. Bogo, and S. Tang. Egobody: Human body shape and motion of interacting people from head-mounted devices. In *Proceedings of the European Conference on Computer Vision (ECCV)*, pp. 180–200, 2022.

## A IMPLEMENTATION DETAILS

### A.1 FEATURE EXTRACTION

Before performing action recognition, we first extract features from all modalities using pre-trained encoders. EEG signals are processed through LaBraM<sup>J</sup>iang et al. (2024), a model pre-trained on 2,500 hours of masked EEG data that generates 2000-dimensional features per channel. Video frames are encoded using VideoMAE<sup>T</sup>ong et al. (2022), pre-trained on EPIC-KITCHENS-100<sup>D</sup>amen et al. (2022), which outputs 1024-dimensional features per segment. During feature extraction, we adopt the parameter settings for EEG features as suggested in Jiang et al. (2024), while the parameters for egocentric video features follow those introduced in Chalk et al. (2024).

### A.2 TOKEN PREPARATION

Before performing action recognition, we first extract features from all modalities using pre-trained encoders (Appendix A.1). To extract aligned segments, Brain-TIM apply a sliding window mechanism with a duration of  $\Delta t$  and step size  $\delta t$ . Each window contains  $N^v = f^v \cdot \Delta t$  video frames and  $N^b = f^b \cdot \Delta t$  EEG samples. The raw data are divided into segments aligned with  $N = \lfloor \frac{T-\Delta t}{\delta t} \rfloor + 1$ , represented as  $V = \{\mathbf{v}_i \in \mathbb{R}^{N^v \times H \times W \times 3}\}_{i=1}^N$  and  $B = \{\mathbf{b}_i \in \mathbb{R}^{N^b \times C}\}_{i=1}^N$ . Below, we detail how to extract feature representations from  $V$  and  $B$ .

**Visual Features:** Within each window in  $V$ , we uniformly down-sample  $K$  frames from their corresponding segment, denoted as  $\{v_1^i, \dots, v_K^i\}$ . The superscript  $i$  refers to the  $i$ -th window, and  $t_i$  is the starting timestamp of the  $i$ -th window, corresponding to the time interval  $[t_i, t_i + \Delta t)$ . The timestamps for each sampled frame are denoted as  $\{\tau_1^i, \dots, \tau_K^i\}$ , where  $\tau_k^i = t_i + \frac{2k-1}{2K} \cdot \Delta t$ , with  $k \in \{1, \dots, K\}$ . This formula ensures that the sampled frames are evenly distributed within the time window and are centered within the window. Each frame is resized to  $224 \times 224$  and normalized using ImageNetDeng et al. (2009) statistics. These  $K$  frames are then passed through a frozen, pre-trained visual encoder  $\phi^v$  to produce a window-level feature vector  $\mathbf{e}^v \in \mathbb{R}^{d^v}$ , where  $d^v$  represents the feature dimension. Combining the sliding stride  $\delta t$ , the full video is encoded into a sequence of window-level feature vectors  $\mathcal{E}^v = \{\mathbf{e}_1^v, \dots, \mathbf{e}_N^v\}$ , where each  $\mathbf{e}_i^v \in \mathbb{R}^{d^v}$ .

**Brain Features:** We adopt a similar sliding window approach to extract neural features from  $B$ . For the  $i$ -th time window, the corresponding EEG signal is denoted as  $\mathbf{b}_i$ . For the raw EEG signal within the window, we first apply a band-pass filter with a range of 0.5–50Hz, followed by downsampling to  $f^b$  Hz. The input  $\mathbf{b}_i$  is fed into a frozen pre-trained encoder  $\phi^b$  to obtain its feature representation  $\phi^b(\mathbf{b}_i) \in \mathbb{R}^{C \times \Delta t \times d^b}$ , where  $d^b$  is the EEG feature dimension. The features are aggregated via channel-wise average pooling as  $\mathbf{e}^b = \frac{1}{C} \sum_{c=1}^C \phi^b(\mathbf{b}_1, \dots, \mathbf{b}_L) \in \mathbb{R}^{\Delta t \times d^b}$ , and temporal pooling is applied when necessary. This produces an aligned sequence of window-level features, denoted as  $\mathcal{E}^b = \{\mathbf{e}_1^b, \dots, \mathbf{e}_N^b\}$ , where each  $\mathbf{e}_i^b \in \mathbb{R}^{d^b}$ . The number of windows  $N$  is kept consistent with the visual modality to ensure temporal alignment between features.

**Token Preparation:** After the features from both modalities are obtained, the learnable embedding layers  $g^v(\cdot)$  and  $g^b(\cdot)$  are applied to  $\mathcal{E}^v$  and  $\mathcal{E}^b$ , respectively, to map modality-specific features into a shared  $D$ -dimensional space. As a result, we obtain the visual feature tokens  $\tilde{\mathcal{E}}^v = \{\tilde{\mathbf{e}}_i^v \in \mathbb{R}^D\}_{i=1}^N$  and the EEG feature tokens  $\tilde{\mathcal{E}}^b = \{\tilde{\mathbf{e}}_i^b \in \mathbb{R}^D\}_{i=1}^N$  without dimension misalignment for further fusion.

To enable cross-modal interaction and support classification for the  $Q$  queries,  $2Q$  learnable classification tokens (`cls` tokens)  $\{\mathbf{c}_i^v \in \mathbb{R}^D\}_{i=1}^Q$  and  $\{\mathbf{c}_i^b \in \mathbb{R}^D\}_{i=1}^Q$  of the same dimension with the feature tokens are introduced for vision and EEG modality, respectively.

### A.3 TRANSFORMER ENCODER

As shown in the Transformer encoder on the right side of Fig. 3, the input sequence  $\mathbf{X}$  is processed by a stack of Transformer encoder layers. Each layer consists of a self-attention mechanism followed by a feedforward network, following the architecture proposed in Vaswani et al. (2017). The self-attention mechanism enables the model to capture long-range dependencies across different positions in the sequence, while the feedforward network applies non-linear transformations to the

input. Each layer uses residual connections and layer normalization to facilitate gradient flow, with the output passed to the next layer to refine the input sequence  $\mathbf{X}$  representations.

#### A.4 LINEAR CLASSIFICATION

Following the Transformer Encoder, as shown in the bottom right of Fig. 3, we extract the modality-specific and query-specific `CLS` tokens from the output sequence. These tokens are fed into their respective classification heads,  $h^v$  and  $h^b$ , which consist of linear layers followed by softmax to produce class probabilities. The two modality branches are trained and evaluated independently, without merging their predicted probabilities into a single unified prediction. The model is supervised using modality-specific cross-entropy losses, denoted as  $\mathcal{L}_v$  and  $\mathcal{L}_b$  for the visual and EEG branches, respectively. The total loss function  $\mathcal{L}$  is defined as the sum of the visual modality loss  $\mathcal{L}_v$  and a weighted term for the EEG modality loss  $\mathcal{L}_b$ , scaled by a hyperparameter  $\lambda$ :  $\mathcal{L} = \mathcal{L}_v + \lambda \cdot \mathcal{L}_b$ .

### B EEG PREPROCESSING PIPELINE

Following LaBraM(Jiang et al., 2024)’s preprocessing pipeline to ensure compatibility across modalities, we first applied a band-pass filter of 0.1–75 Hz to suppress low-frequency noise, followed by a 50 Hz notch filter to eliminate power-line interference. The signals were then resampled to 200 Hz and normalized by scaling the EEG amplitudes from their raw range ( $-0.1$  mV to  $0.1$  mV) to approximately  $-1$  to  $1$ , with  $0.1$  mV set as the unit. Unused or noisy channels were removed to further improve signal quality. Finally, raw EEG recordings (e.g., in `.edf` format) were converted into `HDF5` files to facilitate efficient storage and training.

## C MORE VISUALIZATION

To further illustrate the richness and diversity of the EgoBrain dataset, we provide additional visualizations organized by different subjects (Sec. C.1) and different action categories (Sec. C.2). These examples are intended to help researchers gain deeper insights into the dynamic evolution of multimodal signals across individuals and behaviors within EgoBrain.

#### C.1 VISUALIZATION OF DIFFERENT SUBJECTS

To further illustrate inter-subject variability within the EgoBrain dataset, we present representative initial video frames from all 40 participants in Fig. 6 and Fig. 7. These visualizations clearly demonstrate the abundance of cross-subject samples in EgoBrain, highlighting its strength in capturing individual diversity.

In the initial phase of data collection, we acquired data from 34 participants (P0001–P0034). Following the experimental protocol described in the main paper, we designated data from 22 participants for training, 6 for validation, and the remaining 6 for testing, thereby establishing the “cross-subject only” evaluation setting. Subsequently, to enhance both the diversity of the dataset and the difficulty gradient of the tasks, we collected additional data from 6 participants (P0035–P0040) in different environments. This extended set serves as the foundation for the more challenging “cross-subject & cross-scene” benchmark setting. Overall, the EgoBrain dataset exhibits well-structured diversity across subjects and environments, making it a robust and scalable resource for advancing multimodal brain-computer interface research.

#### C.2 VISUALIZATION OF DIFFERENT ACTION CATEGORIES

To further demonstrate the richness of action categories in the EgoBrain dataset, we provide visualizations covering all 29 annotated action classes. Fig. 8, 9, 10, 11 and , 12 present representative egocentric video frames, highlighting the wide range of daily activities captured in the EgoBrain dataset.

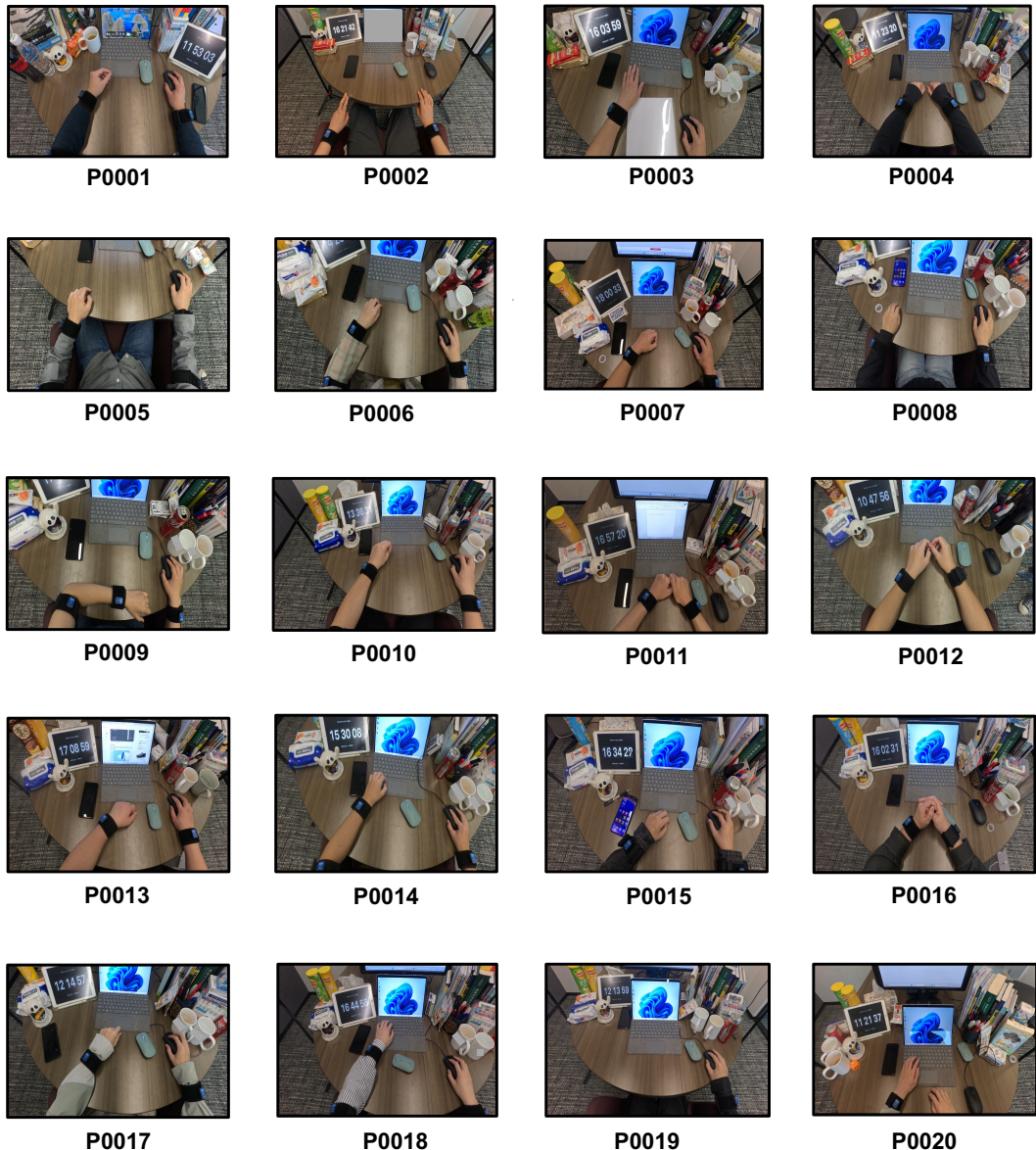


Figure 6: We provide visualizations of initial video frames from participants: P0001 to P0020.

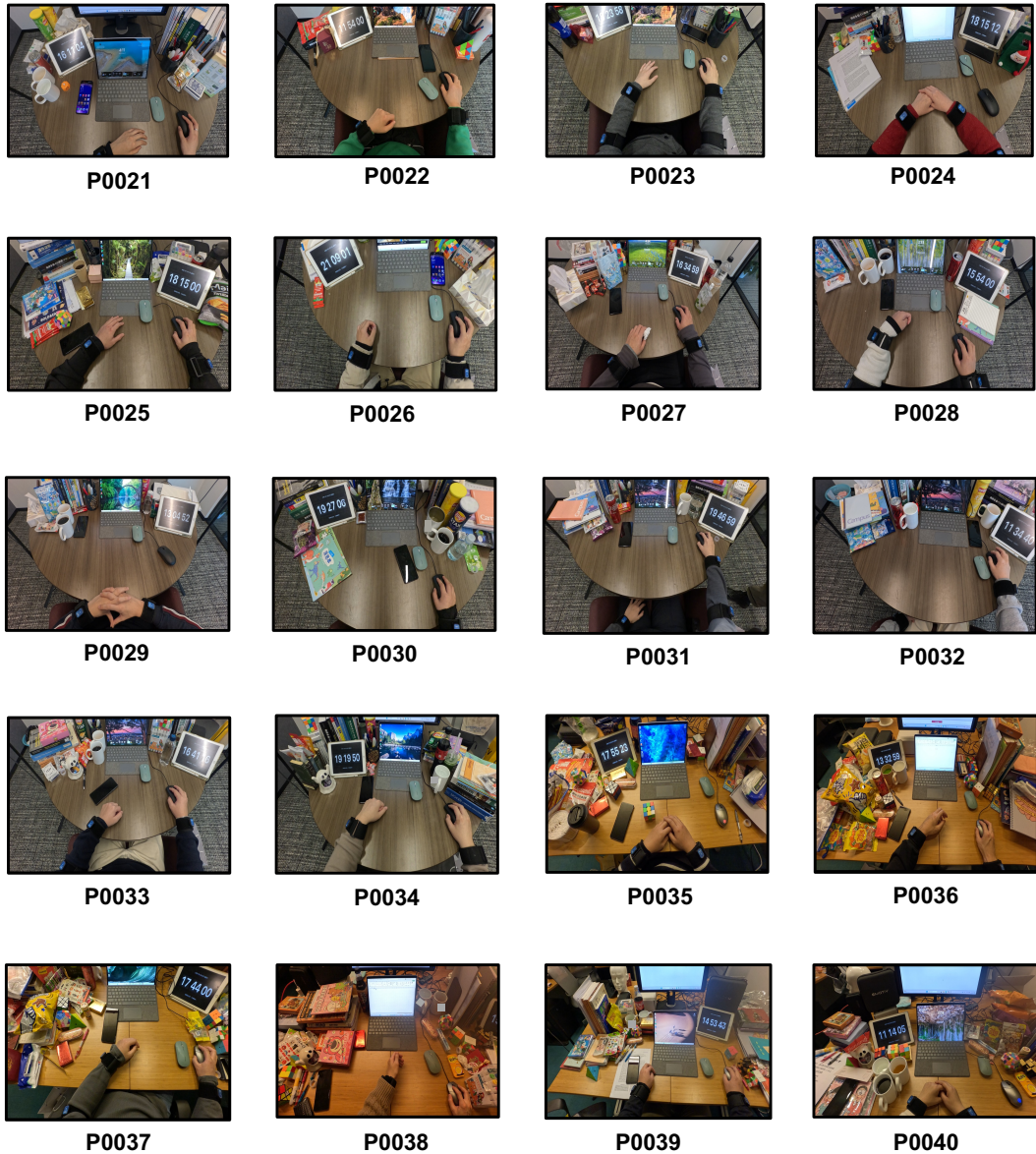


Figure 7: We provide visualizations of initial video frames from participants: P0021 to P0040.

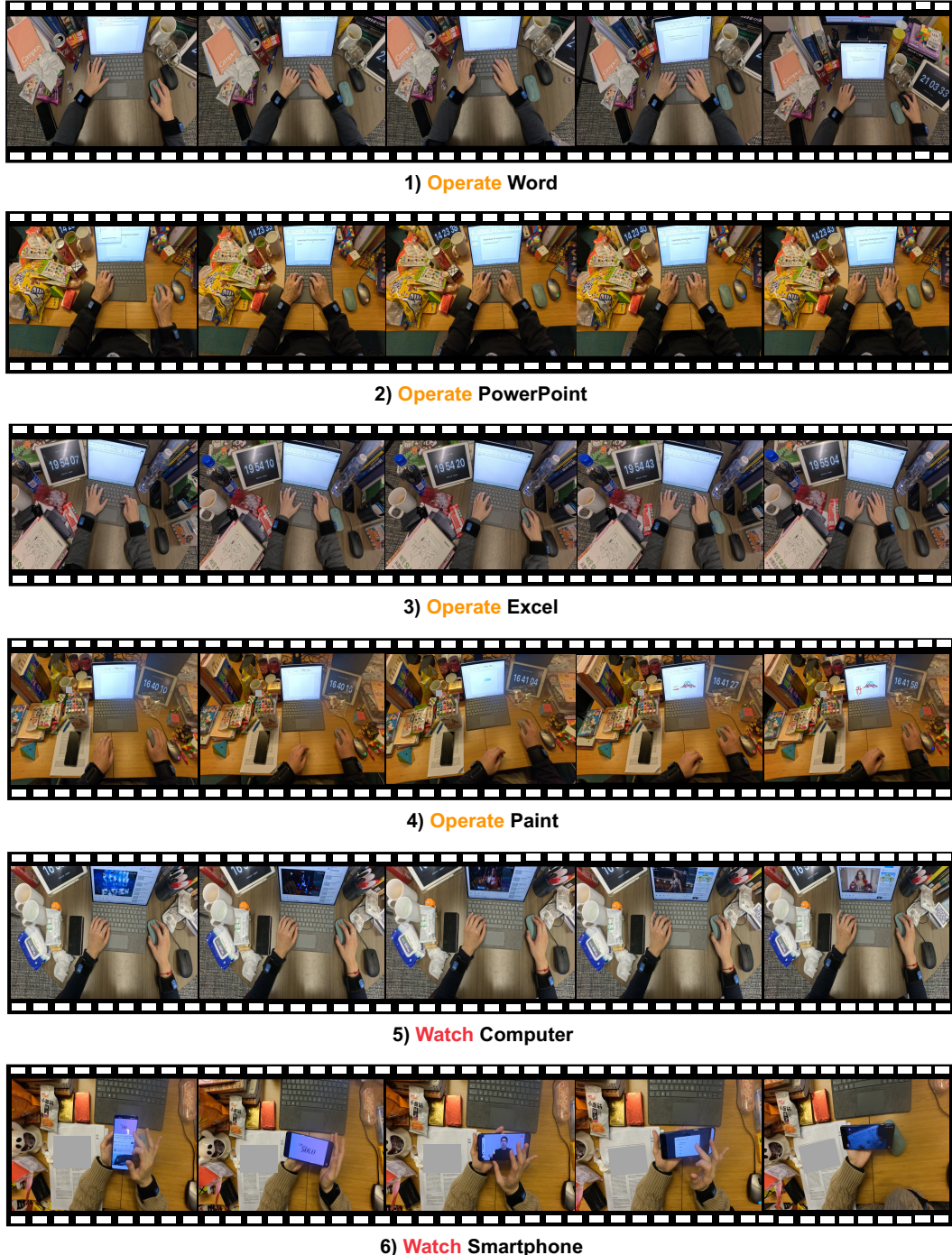


Figure 8: **Visualization of selected action categories including “Operate” and “Watch”.** The egocentric perspective in each sequence offers intuitive insight into the subject’s ongoing motor behavior.

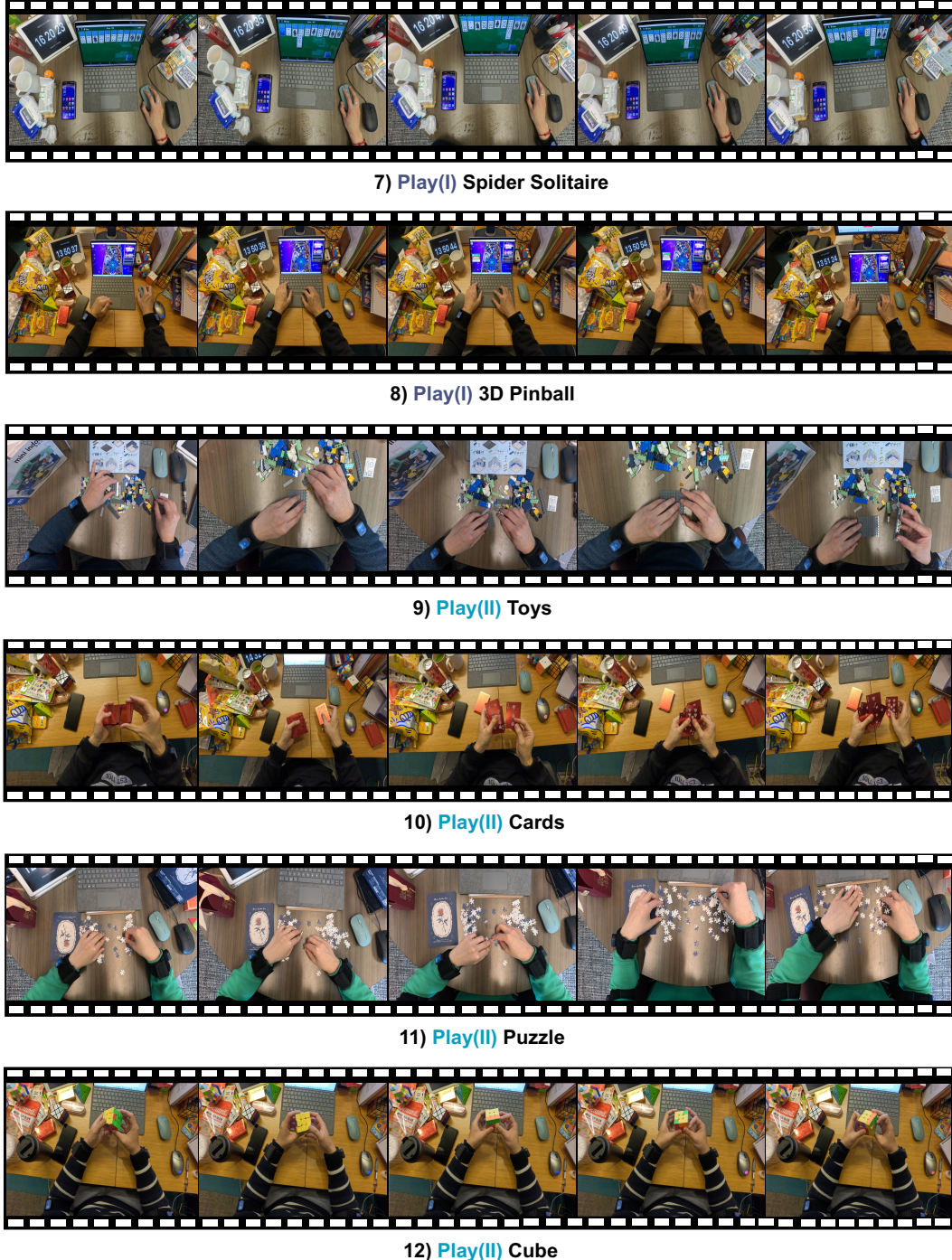


Figure 9: **Visualization of selected action categories including “Play(I)” and “Play(II)”.** The egocentric perspective in each sequence offers intuitive insight into the subject’s ongoing motor behavior.

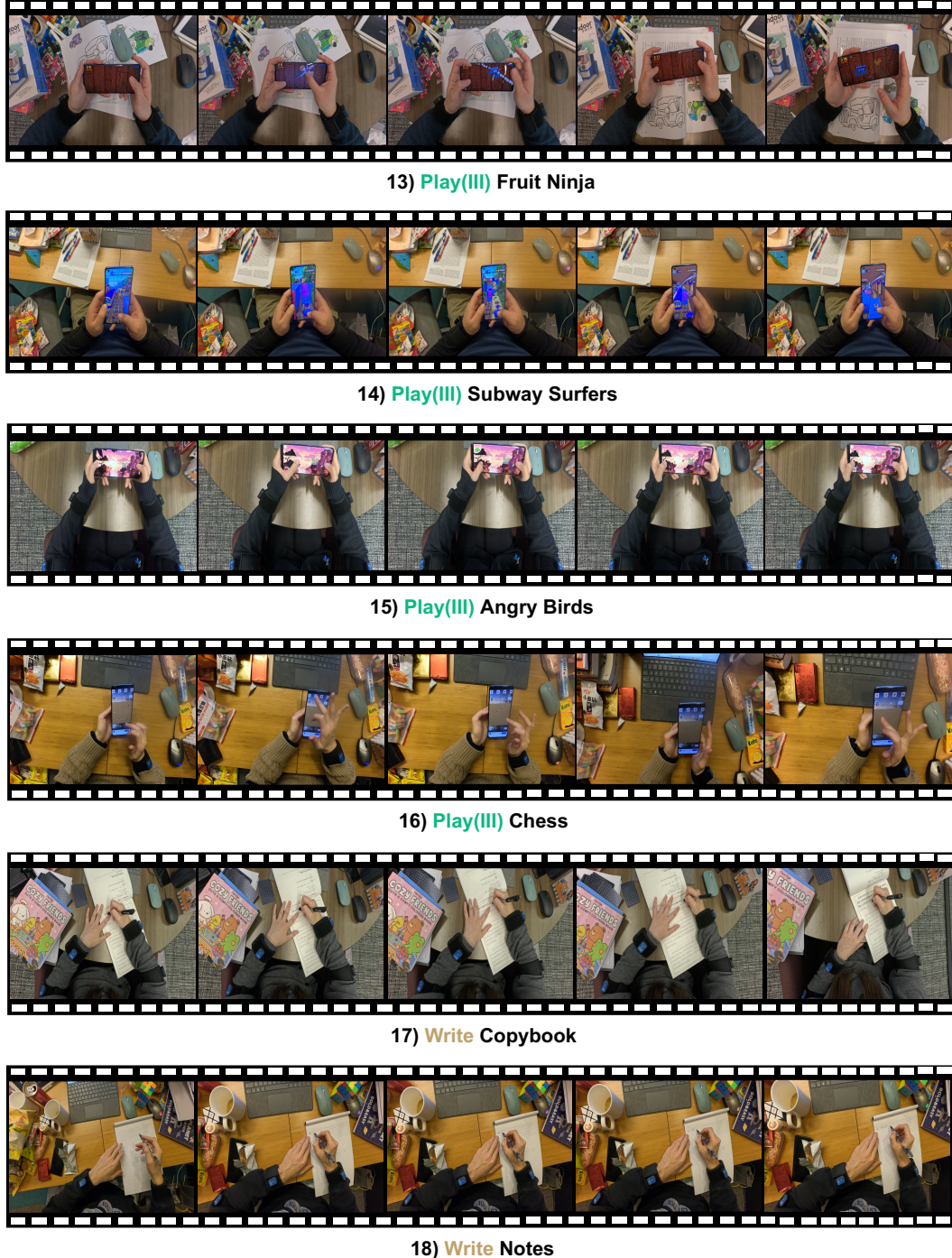


Figure 10: **Visualization of selected action categories including “Play(III)” and “Write”.** The egocentric perspective in each sequence offers intuitive insight into the subject’s ongoing motor behavior.



19) **Read Textbook**



20) **Read Comic book**



21) **Read Research**



22) **Draw Trace**



23) **Draw Pictures**

Figure 11: **Visualization of selected action categories including “Read” and “Draw”.** The ego-centric perspective in each sequence offers intuitive insight into the subject’s ongoing motor behavior.



24) Eat Snack



25) Eat Spicy strips



26) Eat Sugars



27) Drink Water



28) Drink Cola



29) Drink Bitter Gourd Juice

Figure 12: **Visualization of selected action categories including “Eat” and “Drink”.** The egocentric perspective in each sequence offers intuitive insight into the subject’s ongoing motor behavior.